

INSTRUMENTED SOIL REINFORCED RETAINING WALL: ANALYSIS OF MEASUREMENTS

PAOLO CARRUBBA
UNIVERSITA' DI PADOVA, ITALY
NICOLA MORACI
UNIVERSITA' DI REGGIO CALABRIA, ITALY
FILIPPO MONTANELLI
TENAX SPA, ITALY

ABSTRACT

A vertical retaining wall, 4m high and 10m long, was constructed by reinforcing the backfill with geogrids. The reinforcing layers were instrumented with strain gauges, tensile geogrid load transducers and horizontal displacement sensors. In addition, total soil pressure transducers were installed inside the structure to monitor the internal state of stress of the reinforced wall.

The aim of this research is to better understand the behavior of reinforced structures. In particular, the development of slip surfaces and the tensile forces acting in the reinforcements were investigated. By this analysis it was possible to assess current design approaches and related safety factors in terms of either long term tensile failure, pullout, direct sliding or compound failures.

Data related to reinforcement tensile strains and loads, applied vertical pressures, rainfall and construction sequences were collected for two different geogrids over a period exceeding 10,000 hours.

INTRODUCTION

Until now several reinforced structures have been constructed and monitored, but most of them were reinforced with metallic strips since they are easily instrumented. Structures reinforced with geosynthetics are more difficult to be instrumented. Consequently, little data are available on their behavior as loading approaches failure. Therefore, some aspects related to the behavior of these structures remain unclear, including the location and shape of the slip surfaces and the tensile forces acting on the reinforcements.

Several design methods which are based on a limit equilibrium approach have been proposed to address the uncertainties associated with geosynthetic reinforced structures. (Jewell, et al., 1984; Jewell, 1991; Bonaparte, et al., 1987; Broms, 1988; Collin, 1986; Simac, et al., 1990; Leshchinsky and Perry, 1987; Schmertmann, et al., 1987). These methods consider different hypothesis and failure surfaces. So, the factors of safety against failure varies with the design method used.

This paper discusses an instrumented geosynthetic reinforced wall constructed in Italy near the town of Vicenza (Cereda site). The structure was monitored from the initial phase of construction, during the service phase and at failure. Failure was achieved by surcharging the wall with 3.5 m of soil.

This study provides valuable insight in reinforced wall behavior, including the location of failure surfaces, tensile stresses and strains distribution, and factors which can affect short and long term factors of safety such as geosynthetic creep and aging, rain effects and consolidation.

SOIL AND GEOSYNTHETIC PROPERTIES

The soil used for the construction of the wall, is called “Cereda tout venant”, and was excavated from a quarry located near the site of construction. Ten percent of the soil passes the 0.075 mm sieve. It has a uniformity coefficient (C_u) of 130 and a curvature coefficient (C_c) of 19. The grain size distribution is shown in Figure 1. The Atterberg limits were evaluated on the fine fraction and are as follows: liquid limit $LL = 28$, plastic limit $PL = 20$; and plasticity index $PI = 8$. According to the unified soil classification system USCS classification system, this soil is a clayey gravel (GC).

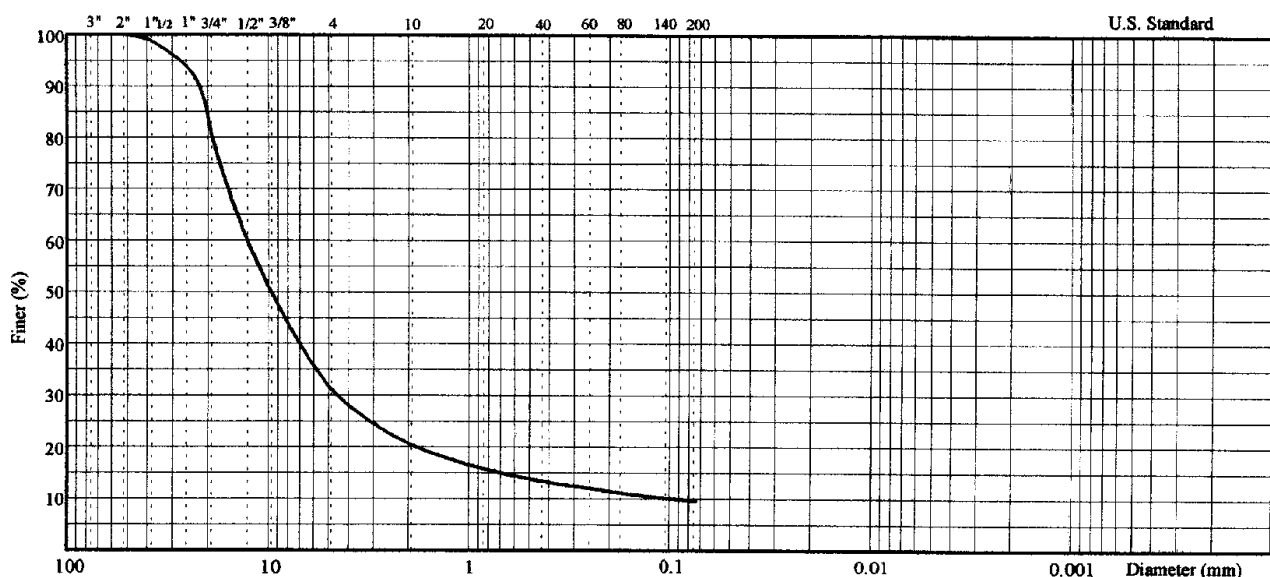


Figure 1. Grain size distribution for the fill soil.

Laboratory compaction tests were carried out following the modified AASHTO method. The results are shown in Figure 2. Maximum dry density ($\gamma_{d \text{ max}}$) values of 22.25 kN/m³ were obtained at an optimum water content (w_{opt}) of 5.5 percent.

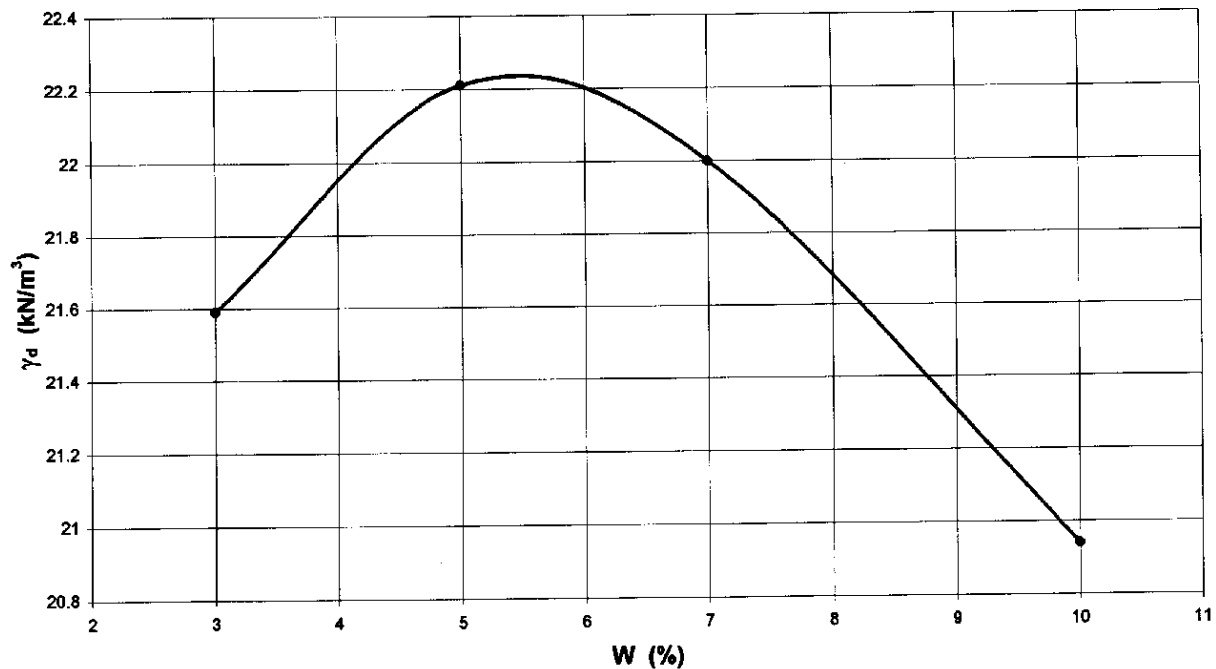


Figure 2. Laboratory compaction test results.

The permeability tests were performed in a triaxial apparatus under constant hydraulic load (corresponding to an hydraulic gradient equal to 1.0) and under confinement pressures of 50 and 100 kPa. The test results of specimens compacted at optimum water content indicate the soil has a permeability coefficient ranging from $2.0 \cdot 10^{-4}$ to $2.5 \cdot 10^{-4}$ cm/s.

To evaluate the soil's shear strength, different laboratory tests were performed. Triaxial tests on large diameter specimens (100 mm) were conducted to determine the shear strength at low strain and confining stress levels. The test results indicate a very high shear strength for confining stresses (σ) between 20 kPa and 100 kPa due to the dilatant behavior of the soil subjected to compaction effort.

Direct shear tests were performed on the portion of soil finer than 0.425 mm using the Casagrande shear box and the Bromhead ring shear apparatus to evaluate its large-displacement shear strength. The tests results indicate a residual shear strength angle (coincident with constant volume shear strength angle Φ_{cv}) of approximately 40 degrees.

The wall was built using two different reinforcement geogrids. One section was 5.0m in

width, and was reinforced with high density polyethylene (HDPE) uniaxial oriented extruded geogrids. The second section was also 5.0m in width and was reinforced with polypropylene (PP) biaxially-oriented extruded geogrids. The geogrids' nominal properties are reported in Table 1.

DESIGN AND CONSTRUCTION

The reinforced wall was designed using a limit equilibrium approach (Leshchinsky 1995) and with the RESLOPE design software. An internal soil friction angle (Φ_{cv}) of 40 degrees was used for the reinforced soil. The two sections of the wall were designed based on two different failure mechanisms: 1) tie-back tensile failure for the portion of wall reinforced with GG20PP geogrids; and 2) pullout failure for the other portion reinforced with GG45PE geogrids. The design parameters used are listed in Table 2. All the Safety Factors were deliberately set to 1.00 to design a wall at limit equilibrium stage and consequent failure during surcharge loading.

Table 1. Geogrids' nominal properties.

Product Name	Tenax LBO 220 SAMP	Tenax TT 201 SAMP
Product Code	GG20PP	GG45PE
Polymer Type	Polypropylene	High Density Polyethylene
Nominal Tensile Strength, MD	20 kN/m	45 kN/m
Strain at Peak, MD	11%	12%
Tensile Strength at 2% Strain	7 kN/m	13 kN/m
Tensile Strength at 5% Strain	14 kN/m	26 kN/m
Unit Weight	270 g/m ²	450 g/m ²
Mesh Sizes	41 x 31 mm	130 x 15 mm
Junction Strength	18 kN/m	36 kN/m

The long term allowable design tensile strength of the geogrids was assumed to be equal its peak tensile strength as determined by the wide width tensile test method (ASTM D4595). Since geogrids with different strengths were used in the designs, the vertical spacing and reinforcement lengths of these two sections were also different. For the section reinforced with GG20PP geogrids, three layers, each 2.20m long, were necessary. The first layer was installed at elevation 0.00m with respect to the base, the second at 0.80m and the third at 2.40m elevation. For the section reinforced with GG45PE geogrids, three layers, each 2.00m long, were necessary. The first layer was installed at elevation 0.00m with respect to the base, the second at 1.30m and the third at 2.90m elevation.

Table 2. Retaining wall design parameters.

GEOMETRY AND LOADING DATA	
• Height of the slope, H (m)	4.0
• Height of soil surcharge at failure, H (m)	3.5
• Face inclination, β	85°
FACTORS OF SAFETY	
• Factor of safety for direct sliding	1.0
• Factor of safety for geosynthetic uncertainties	1.0
• Factor of safety for geosynthetic pullout	1.0
• Factor of safety for installation damage	1.0
• Factor of safety for chemical degradation	1.0
• Factor of safety for biological degradation	1.0
• Factor of safety for creep	1.0
INTERACTION COEFFICIENTS	
• Pullout interaction coefficient	0.9
• Direct sliding coefficient	1.0

To ensure the face stability and geometry, the structure was constructed using “left in place” welded wire formworks. They are composed of wire mesh precut to an height of about 1.5m and bent to the face at an angle of 85 degrees. The fill soil was compacted in layers of 0.3m thick using a vibrating roller (80 kN). The structure is shown in Figure 3.



Figure 3. View of the two reinforced walls.

The geogrids were instrumented with self-temperature compensated strain gauges having a nominal gauge length of 5mm and a maximum strain of 10% with a measurement accuracy of 0.5%. The strain gauges were glued to the geogrid ribs with cyanoacrylate adhesive using a multi-step method. This procedure allows the measurement of the geogrid strains up to 10%, over a period in excess of two years and during freezing temperatures. Ten strain gauges were installed on each reinforcement layer at a spacing of about 0.20m. The strain gauges were protected with silicon rubber and with a 0.10m-thick sand layer. The effectiveness of this procedure has been demonstrated by the low mortality rate of the sensors (only one out of 63 sensors malfunctioned). The electrical connection was made using a three wires Whetstone quarter bridge. The strain gauges were connected to an automatic data acquisition unit which is capable of recording up to 100 sensors every 15 minutes. The actual recording frequency was reduced to once per day after the construction was completed. Additional specimens of geogrids, were instrumented with strain gauges, were prepared and tested in the laboratory to provide a basis for calibration and correlation between strain and tensile stress. The stress-strain curves and modulus for both geogrids were established with laboratory testing. These relationships are function of time, temperature, stress and strain. The following tests were performed to define the time dependent properties of the geogrids: in isolation index single rib tensile tests, low strain rate tensile tests, and different load ratio creep tests.

Three tensile load cells, each having a physical profile similar to the shape of the uniaxial geogrid, were installed at each GG45PE reinforcement layer to record the actual confined tensile loads in the material. Three vertical total stress cells, each having a diameter of 300mm, were installed at each GG45PE reinforcement layer to record the actual vertical total stress in soil. These cells were located 1m inside the wall face. Horizontal multiple base displacements sensors were installed on the GG45PE geogrid layers to monitor absolute and differential movements of the reinforced mass and its face.

ANALYSIS OF THE RECORDED DATA

The change of total vertical pressures over time at the different reinforcing layers during construction and surcharging is shown in Figure 4 for the section of wall reinforced with GG45PE. These data demonstrate a good response of instrumentation to the vertical pressure changes, even if some discrepancies may be noticed with respect to theoretical values. This behavior may be attributed to the proximity of the cells to face (1.0m), the flexibility effects of the face itself, the position of the cells with respect to the surcharge and finally, to the presence of a rigid base on which the wall was founded.

The change of the total vertical pressures over time are compared to the recorded rainfall in Figure 5. The figure shows that the change of the unit weight over time has a little influence on recorded data. A comparison between the applied total vertical pressures and the associated strains in reinforcing layers is shown in Figure 6 for both geogrids. This comparison is made for selected points (Table 3) which are approximately at the same position with respect to the wall

face. The data in Figures 4 & 5 indicates a good response with respect to time of loading of the two independent monitoring systems. For a given stress level, the dependence of recorded strain on geogrid stiffness is clearly shown in Figure 6.

Figure 7 shows the development of tensile strain over time in the upper layer of both GG45PE and GG20PP. The data indicate a marked dependence of the tensile strain in geogrids on the stress level achieved during surcharging, the geogrid stiffness and its creep properties. Moreover, for a given temperature, creep became more important as the tensile stress in reinforcement increases. Finally, it is possible to observe that the effect of creep is more significant in GG20PP geogrids than in GG45PE geogrids. This is due to the different polymer, manufacturing process, and the involved failure mechanisms. The development of tensile strains over time for strain gauges located at different locations is shown Figures 8 and 9 for the GG20PP and the GG45PE geogrids, respectively.

Table 3. Designation and location of strain gauges installed on reinforcing geogrids.

GG45PE						GG20PP					
Channel N. Vs. Face Distance, m						Channel N. Vs. Face Distance, m					
BASE		MEDIUM		UPPER		BASE		MEDIUM		UPPER	
CH 11	0.06	CH 21	0.18	CH51	0.07	CH 01	0.10	CH 41	0.10	CH 31	0.16
CH 12	0.21	CH 22	0.45	CH52	0.35	CH 02	0.32	CH 42	0.29	CH 32	0.39
CH 13	0.35	CH 23	0.73	CH53	0.63	CH 03	0.54	CH 43	0.49	CH 33	0.83
CH 14	0.49	CH 24	1.01	CH54	0.77	CH 04	0.77	CH 44	0.70	CH 34	1.06
CH 15	0.62	CH 25	1.12	CH55	0.90	CH 05	1.00	CH 45	0.91	CH 35	1.29
CH 16	0.76	CH 26	1.30	CH56	1.04	CH 06	1.23	CH 46	1.13	CH 36	1.52
CH 17	0.90	CH 27	1.45	CH57	1.18	CH 07	1.46	CH 47	1.34	CH 37	1.72
CH 18	1.17	CH 28	1.59	CH58	1.32	CH 08	1.69	CH 48	1.54	CH 38	1.95
CH 19	1.45	CH 29	1.73	CH59	1.46	CH 09	1.92	CH 49	1.74	CH 39	2.05
CH 20	1.73	CH 30	1.88	CH60	1.73	CH 10	2.06	CH 50	1.94	CH 40	----

The maximum tensile strain achieved in each reinforcing layer indicates the location in which tension is greatest. Using this information, the location of the internal failure plane can be identified. The two slip surfaces obtained by this analysis are shown in Figures 10 and 11 as well as the failure surfaces considered in the design step, and the tensile strains measured. Moreover, the data in Figures 10 and 11 indicate that the reinforcing layers are stressed in a different way.

The actual mechanism of failure for GG45PE is pullout, as indicated by the multibase displacement data and by the low values of measured tensile strains (0.6-1.6% in Figure 9). The actual failure mechanism for GG20PP is tensile stress in the upper reinforcing layer as indicated by the high tensile strains measured (about 4.0 percent in Figure 8).

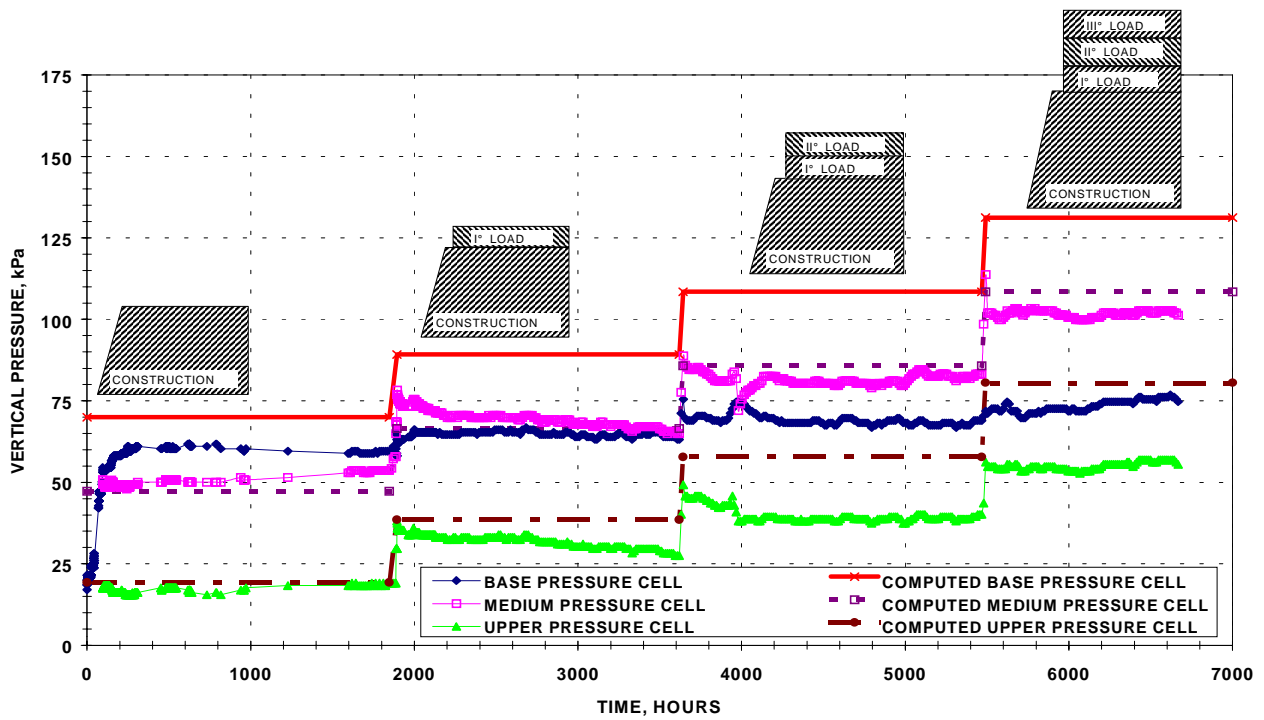


Figure 4. Variation of total vertical pressure during construction and surcharging for the GG45PE geogrid reinforced wall.

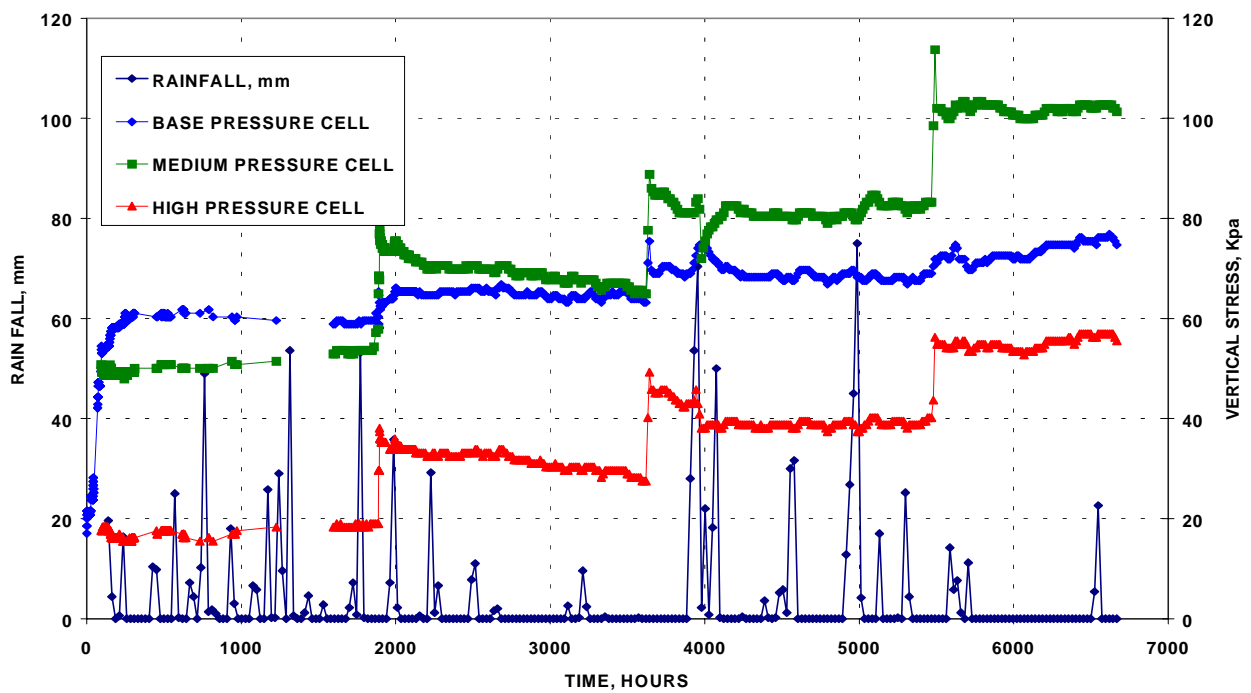


Figure 5. Total vertical pressure and rainfall during construction and surcharging for the GG45PE geogrid reinforced wall.

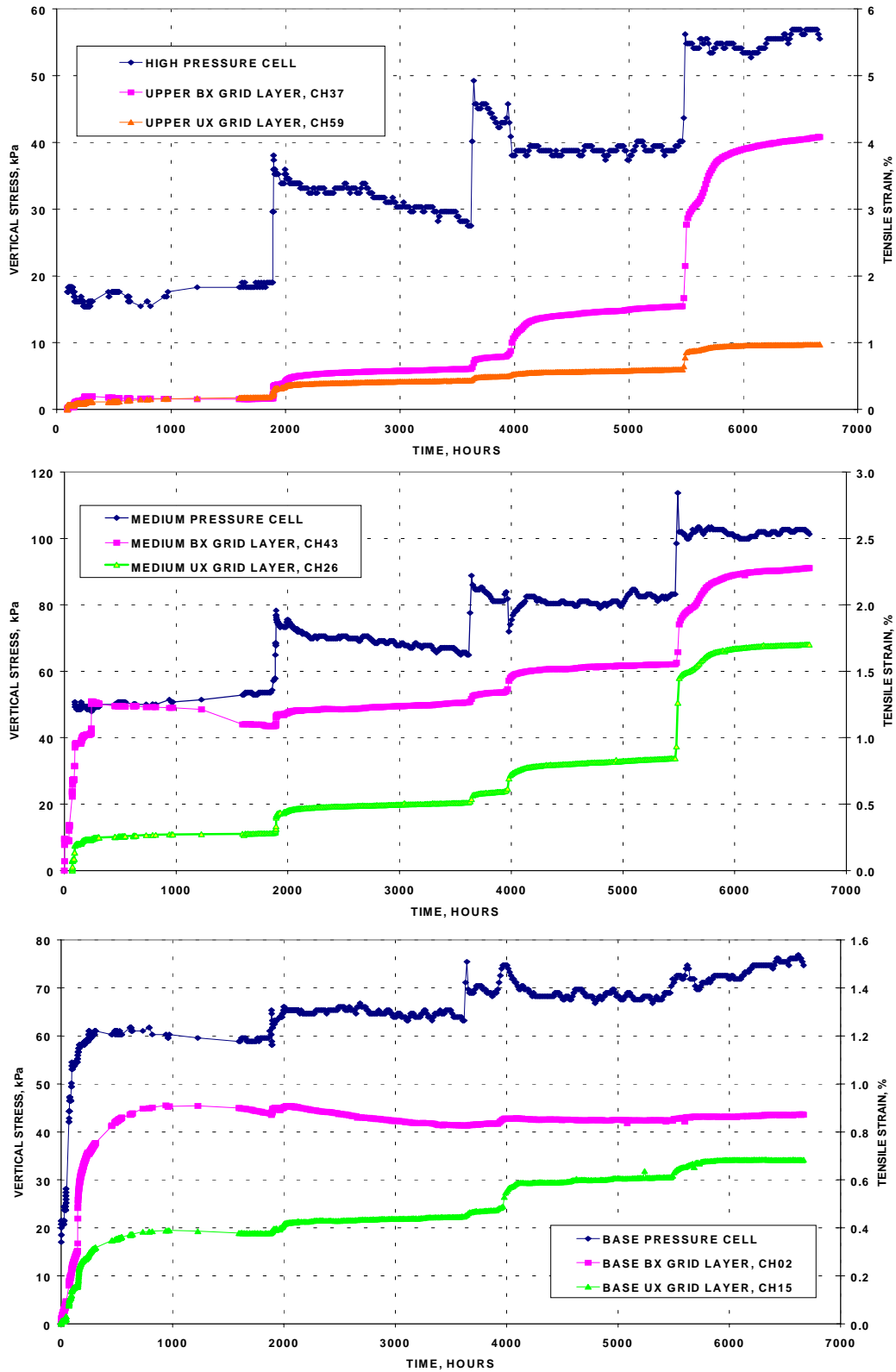


Figure 6. Comparison between total vertical pressure and strains at some instrumented locations of the GG45PE and the GG20PP geogrids.

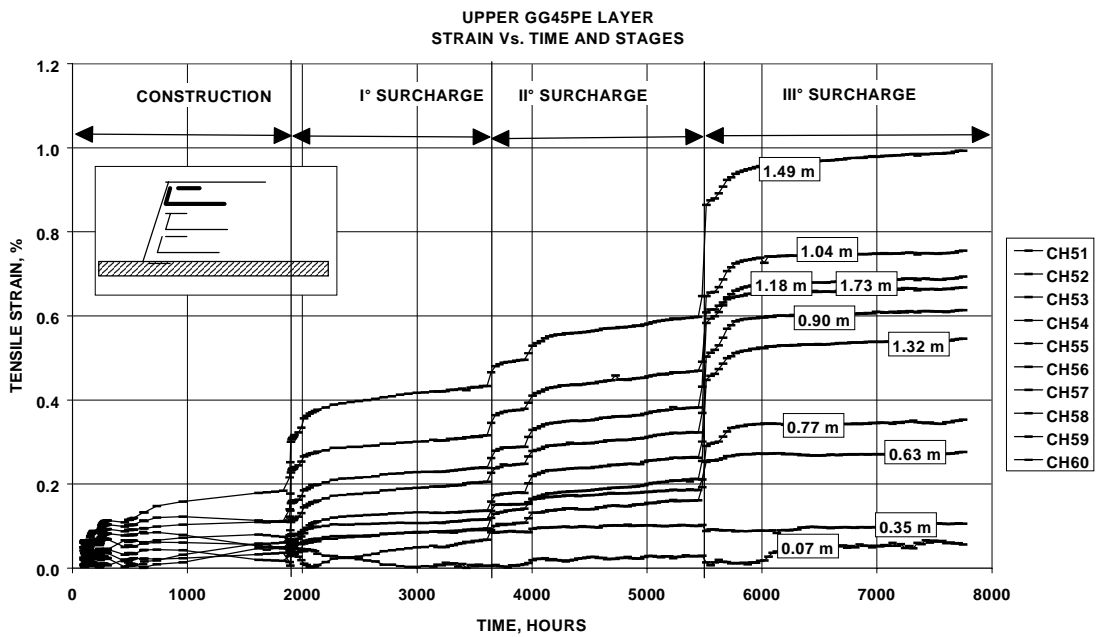
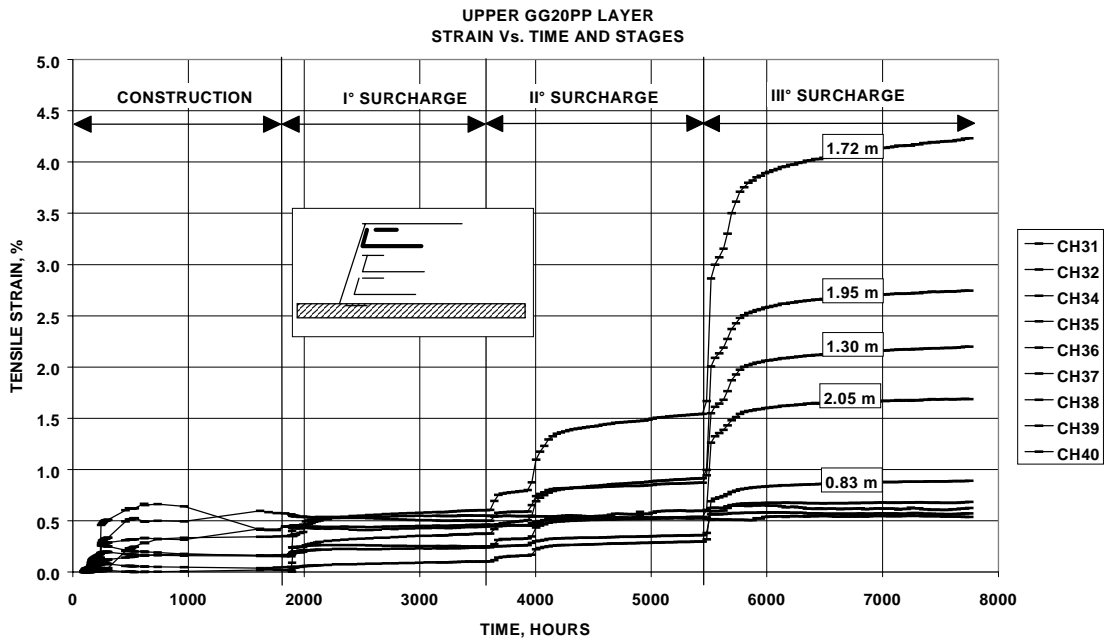


Figure 7. Tensile strains vs. time in the upper reinforcing layers for the GG45PE and the GG20PP geogrids. On the curves are shown the strain gages face distance (Table 3).

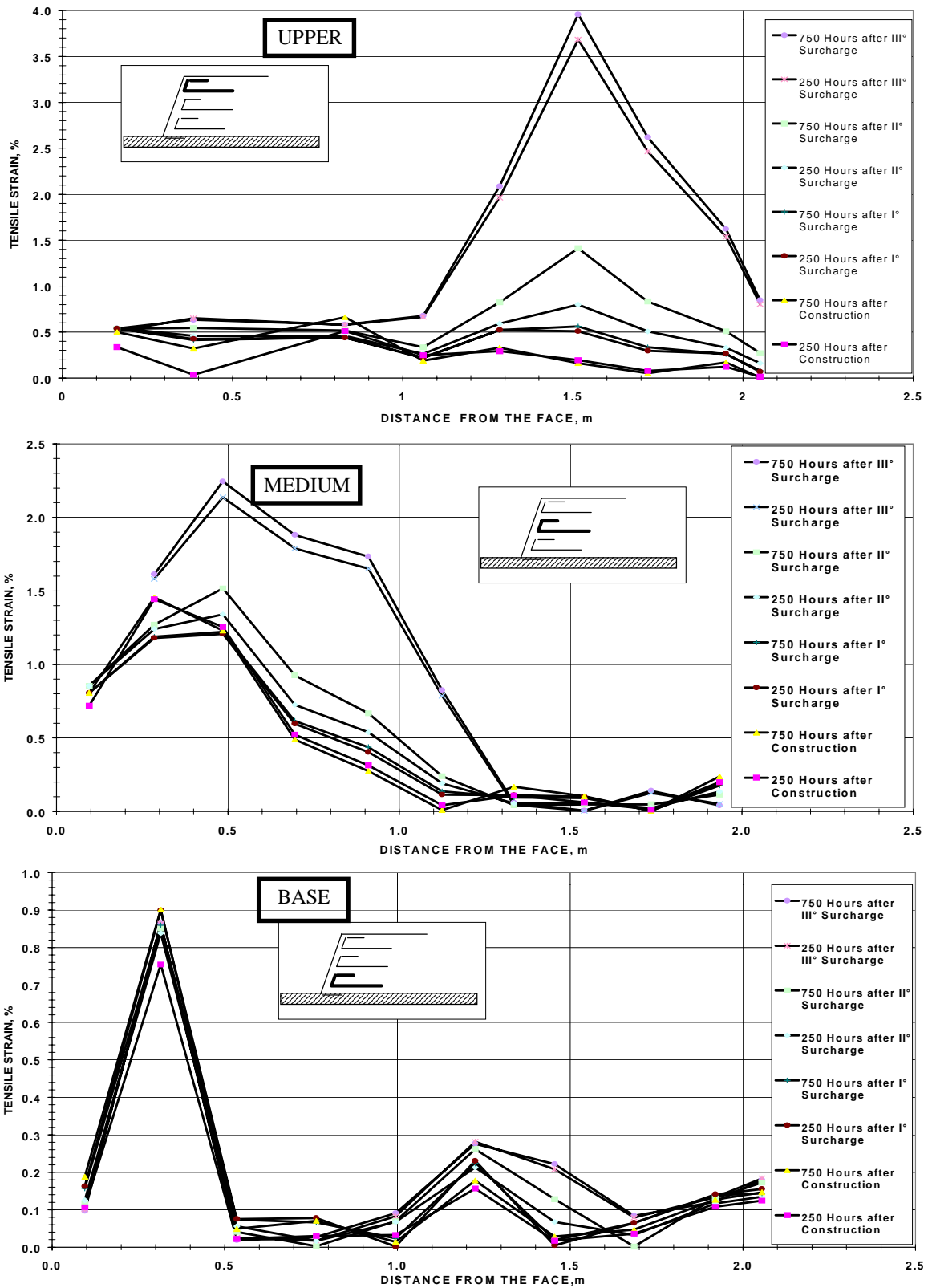


Figure. 8 Tensile strains vs. time along the GG20PP geogrid reinforcing layers.

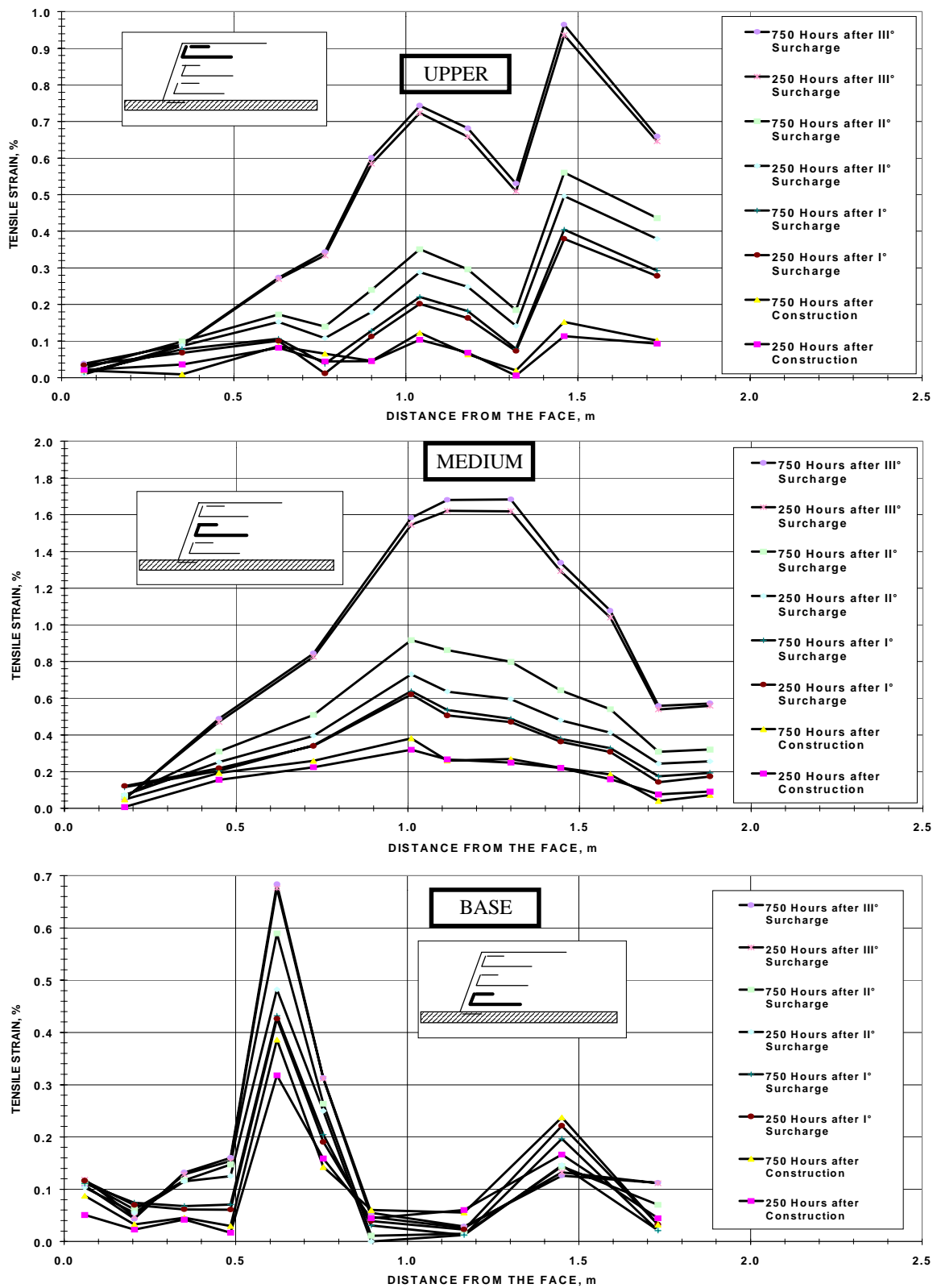


Figure 9. Tensile strains vs. time along the GG45PE geogrid reinforcing layers.

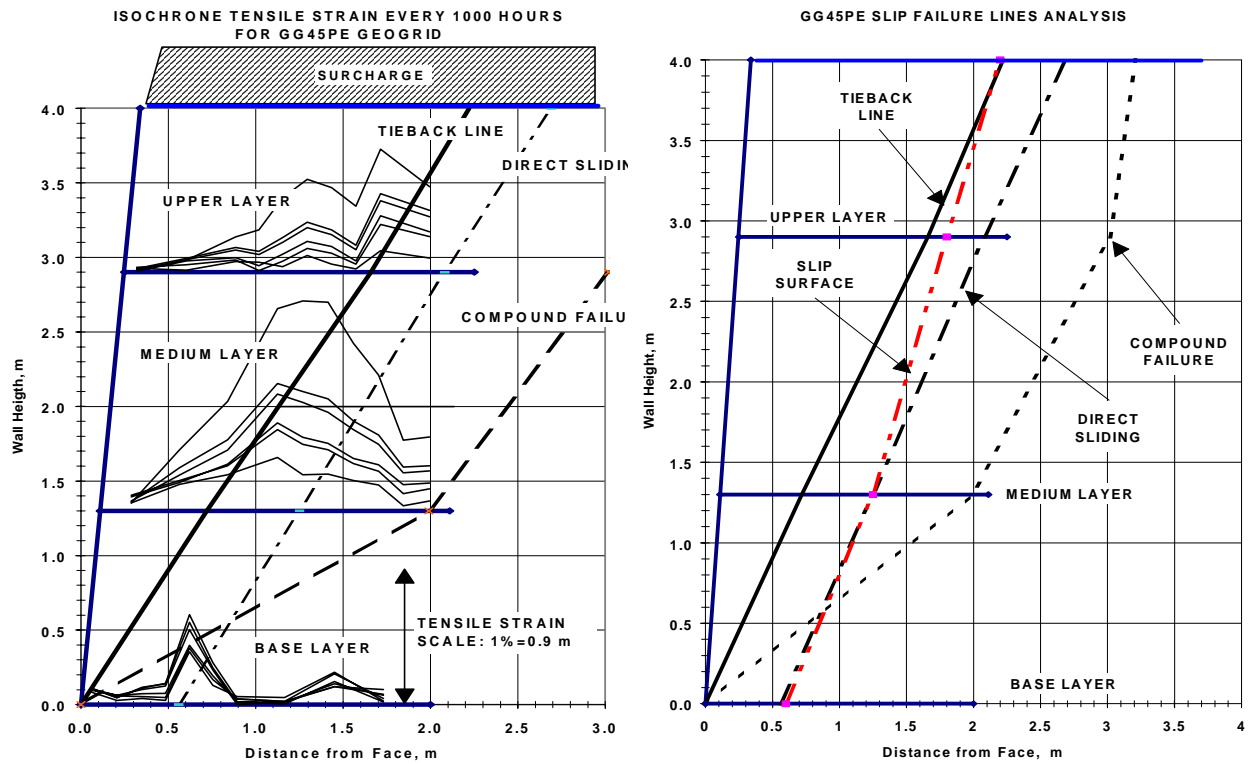


Figure 10. Localization of the actual slip surfaces inside the GG45PE reinforced wall.

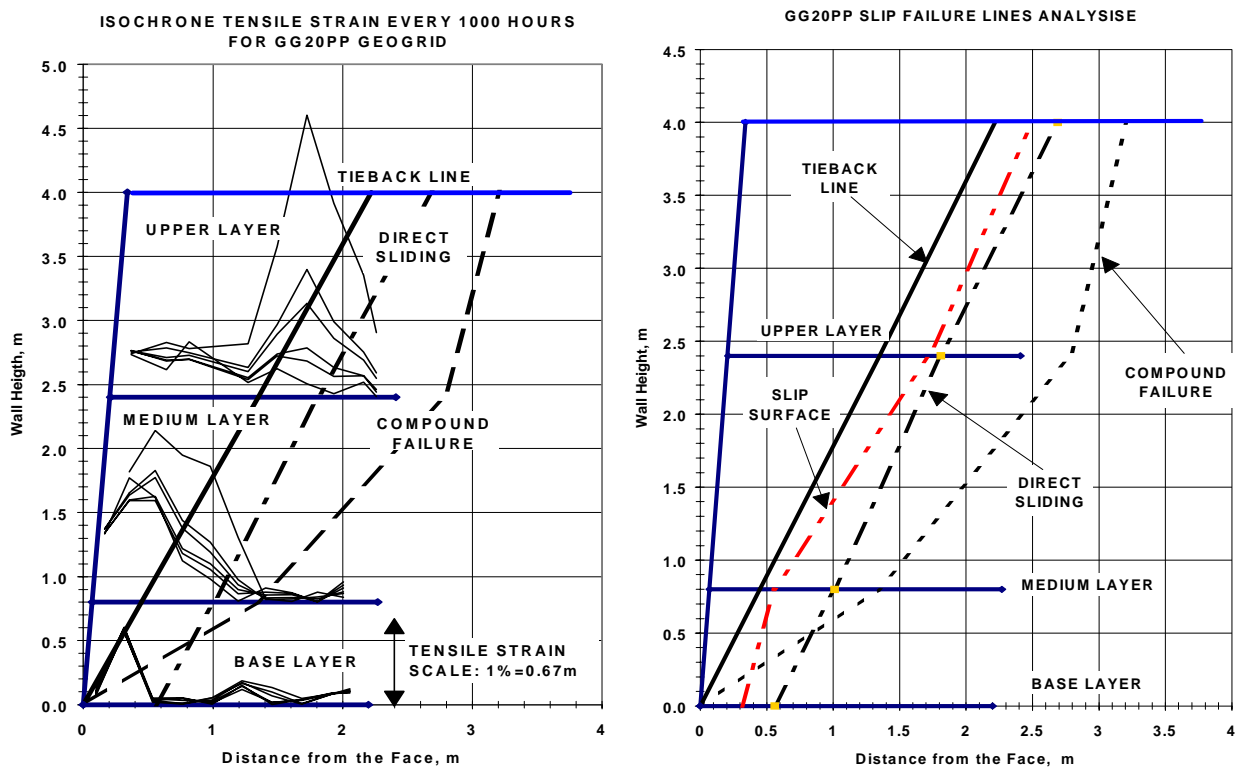


Figure 11. Localization of the actual slip surfaces inside the GG20PP reinforced wall.

CONCLUSIONS

A vertical retaining wall, 4m high and 10m long, was constructed by reinforcing the backfill with two different type of geogrids. The reinforcing layers were instrumented with strain gauges, tensile geogrid load transducers and horizontal displacement sensors. Moreover, in order to measure the internal state of stress of the reinforced walls, total soil pressure transducers were installed inside the structure. Finally, the walls were brought to failure by surcharging with 3.50m of loose soil. The tensile strains collected inside the reinforced structures allowed the location of failure surfaces to be clearly identified. Two different failure mechanisms were identified: a pull-out mechanism failure, in the case of GG45PE reinforced wall, and a tensile reinforcing failure, in the case GG20PP reinforced wall. The paper shows that the instrumentation and the long term observation of a large scale model may be considered a valuable tool in understanding the behavior of such a complex structures.

REFERENCES

- Bonaparte, R., Holtz, R.D. and Giroud, J.P. (1987) “ Soil Reinforcement Design Using Geotextiles and Geogrids”, Geotextile Testing and the Design Engineer, ASTM STP 952, pp.69-116.
- Collin, J.G. (1986) “ Earth Wall Design”, Ph.D. Thesis, University of California, Berkley; U.S.A.
- Jewell, R.A (1991) “ Application of Revised Design Charts for Steep Reinforced Slopes ”, Geotextiles and Geomembranes, Vol.10, n.4, pp.203-233.
- Jewell, R.A., Paine, N., Woods, R.I. (1984) “ Design Method for Steep Reinforced Embankments ”, Polymer Grid Reinforcement in Civil Engineering, Thomas Telford, London, U.K., pp.70-81.
- Leshchinsky, D., Perry, E.B. (1987) “ A Design Procedure for Geotextile-Reinforced Walls ”, Proceeding Geosynthetic '87, New Orleans, U.S.A., pp.95-107.
- Leshchinsky, D. (1995) “ RESLOPE ” Design Manual, Department of Civil Engineering , University of Delaware, U.S.A.
- Schmertmann, G.R., Chouery-Curtis, V.E., Johnson, R.D. and Bonaparte, R. (1987) “ Design Charts for Geogrid-Reinforced Soil Slopes ”, Proceeding Geosynthetic '87, New Orleans, U.S.A., pp.108-120.
- Simac, M.R., Christopher, B.R., and Bonczkiewicz, C. (1990) “ Instrumented Field Performance of a 6 m Geogrid soil wall ” Proceeding 4th International on Geotextiles Geomembranes and Related Products, The Haughe, Holland, Vol.1, pp.53-59.